

Dimer-dimer collisions at finite energies in two-component Fermi gases

J. P. D’Incao, Seth T. Rittenhouse, N. P. Mehta, and Chris H. Greene

Department of Physics and JILA, University of Colorado, Boulder, Colorado 80309-0440, USA

We introduce a major theoretical generalization of existing techniques for handling the three-body problem that accurately describes the interactions among four fermionic atoms. Application to a two-component Fermi gas accurately determines dimer-dimer scattering parameters at finite energies and can give deeper insight into the corresponding many-body phenomena. To account for finite temperature effects, we calculate the energy-dependent *complex* dimer-dimer scattering length, which includes contributions from elastic and inelastic collisions. Our results indicate that strong finite-energy effects and dimer dissociation are crucial for understanding the physics in the strongly interacting regime for typical experimental conditions. While our results for dimer-dimer relaxation are consistent with experiment, they confirm only partially a previously published theoretical result.

PACS numbers: 31.15.xj,34.50.-s,34.50Cx,67.85.-d

The physics of strongly interacting fermionic systems is of fundamental importance in many areas of physics encompassing condensed matter physics, nuclear physics, particle physics and astrophysics. The last few years have seen extensive theoretical and experimental efforts devoted to the field of ultracold atomic Fermi gases. The ability to control interatomic interactions through magnetically tunable Feshbach resonances has opened up broad vistas of experimentally accessible phenomena, providing a quantum playground for studying the strongly interacting regime. For instance, near a Feshbach resonance between two dissimilar fermions, the *s*-wave scattering length a can assume positive and negative values, allowing for the systematic exploration of Bose-Einstein condensation (BEC) and the Bardeen-Cooper-Schrieffer (BCS) crossover regime, in which bosonic ($a > 0$) and fermionic ($a < 0$) types of superfluidity connect smoothly [1, 2]. In this broad context, few-body correlations [3, 4] play an important role in describing the dynamics of such systems. On the BEC side of the resonance ($a > 0$), dissimilar fermions pair-up into weakly-bound bosonic dimers, and the zero (collision) energy dimer-dimer scattering length, $a_{dd}(0)$, determines various experimental observables such as the molecular gas collective modes, the internal energy, and even the macroscopic spatial extent of the confined cloud [1, 2]. Although a better description of the many-body behavior has emerged through the inclusion of few-body correlations, most of the current understanding of crossover physics relies on zero-energy theories, and very little is known about finite energy effects in this regime (see Ref. [5] and references therein).

In this Letter we demonstrate important finite energy effects which can potentially impact the physics of a finite temperature ultracold Fermi gas in the crossover regime. Our results show deviations from zero-energy dimer-dimer collisions and indicate that, at experimentally relevant temperatures and scattering lengths, molecular dissociation might play an important role. The crossover regime can be viewed as a long-lived atom-molecule mixture, where dimers are dynamically converted to atoms and vice-versa. In order to account for finite tempera-

ture effects, we calculate the energy dependent *complex* dimer-dimer scattering length, $a_{dd}(E_{col})$, where E_{col} is the collision energy. The real and imaginary parts of a_{dd} correspond, respectively, to contributions from elastic and inelastic (dissociative) collisions [6], both of which should be considered to properly model the Fermi gas at realistic temperatures. In the zero-energy limit we reproduce the well known prediction $a_{dd}(0) \approx 0.6a$ [4]. However, when the dimer binding energy, $E_b = \hbar^2/(2\mu_{2b}a^2)$ (where μ_{2b} is the two-body reduced mass) is comparable to the gas temperature T , finite energy effects and molecular dissociation become important, defining a critical scattering length $a_c = \hbar/(2\mu_{2b}k_B T)^{1/2}$, where k_B is Boltzmann’s constant, beyond which an atom-molecule mixture should prevail.

We also study dimer-dimer relaxation, in which two weakly-bound dimers collide and make an inelastic transition to a lower energy state. In such a process, the kinetic energy released is enough for the collision partners to escape from typical traps. Ref. [4] predicted that, near a Feshbach resonance, dimer-dimer relaxation is suppressed as $a^{-2.55}$, explaining the long lifetimes observed in several experiments [2, 7]. Here we also verify this suppression, although with an a dependence that is not described as a simple power-law scaling as originally predicted [4]. While the $a^{-2.55}$ scaling law has already been tested (Regal *et al.* [7] found $a^{-2.3 \pm 0.4}$ and Bourdel *et al.* [2] $a^{-2.0 \pm 0.8}$), our calculations demonstrate that finite range corrections can explain the apparent experimental scaling law behavior, despite deviations from that power-law for larger a .

We solve the four-body Schrödinger equation in the hyperspherical adiabatic representation, which offers a simple yet quantitative picture. A finite range model is assumed for the interatomic interaction, and a physically-motivated variational basis set is adopted to solve the hyperangular equations [8]. While several hyperangular parameterizations exist, we find that the best choice is the “democratic” hyperspherical coordinates [9] in which all possible fragmentation channels are treated on an equal footing, which describes elastic and inelastic processes in an unified picture.

In the adiabatic hyperspherical representation, the collective motion of the four fermions is described in terms of the hyperradius R , characterizing the overall size of the system. The interparticle relative motion is described by the hyperangles $\Omega \equiv \{\theta_1, \theta_2, \phi_1, \phi_2, \phi_3\}$, and the set of Euler angles $\{\alpha, \beta, \gamma\}$ specifying the orientation of the body-fixed frame [9]. θ_1 and θ_2 parameterize the moments of inertia while ϕ_1, ϕ_2 and ϕ_3 parameterize internal configurations [9]. Integrating out the hyperangular degrees of freedom, the Schrödinger equation reduces to a system of coupled ordinary differential equations, given in atomic units (used throughout this Letter) by:

$$\left[-\frac{1}{2\mu} \frac{d^2}{dR^2} - E \right] F_\nu(R) + \sum_{\nu'} W_{\nu\nu'}(R) F_{\nu'}(R) = 0, \quad (1)$$

where $\mu = m/4^{1/3}$ is the four-body reduced mass (m being the atomic mass), E is the total energy, F_ν is the hyperradial wavefunction, and ν represents all quantum numbers needed to label each channel. Scattering observables can then be extracted by solving Eq. (1), where the nonadiabatic couplings $W_{\nu \neq \nu'}$ drive inelastic transitions between channels described by the effective potentials $W_{\nu\nu}$.

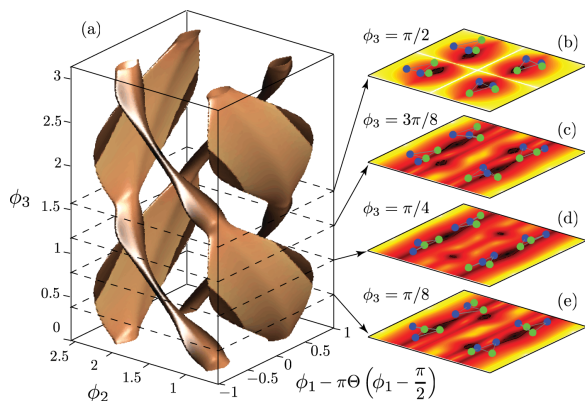


FIG. 1: (color online). Analysis of the probability density integrated over the hyperangles θ_1 and θ_2 at $R = 0.41 a$ is shown. (a) An isosurface of the probability density at $|\Phi(R; \Omega)|^2 = 0.1 |\Phi(R; \Omega)|_{\max}^2$ for the dimer-dimer channel is shown. The darker (lighter) colors correspond to a more (less) linear configuration for the four-particle system. $\Theta(x)$ is the unit-step function. (b)-(e) show density plots for fixed values of ϕ_3 . The darker regions represent higher probabilities for which planar configurations are shown to illustrate the most probable four-body geometry at selected points.

In the hyperspherical representation, the major reduction to Eq. (1) is accomplished by finding eigenfunctions of the (fixed R) adiabatic Hamiltonian,

$$\hat{H}_{\text{ad}}(R, \Omega) = \frac{\hat{\Lambda}^2(\Omega) + 12}{2\mu R^2} + \hat{V}(R, \Omega). \quad (2)$$

In the above equation, $\hat{\Lambda}$ is the grand angular momentum operator [9] and \hat{V} includes all two-body interactions [10]. For simplicity, we neglect the interaction between

identical fermions and assume the one between dissimilar fermions to be $v(r) = D \text{sech}^2(r/r_0)$, where r is the interatomic distance and D is tuned to produce the desired a . We choose the atomic mass m and effective range $r_0 = 181$ a.u. [11] to be those of ^{40}K . The eigenvalues and eigenfunctions of \hat{H}_{ad} , namely the hyperspherical potentials $U_\nu(R)$ and channel functions $\Phi_\nu(R; \Omega)$, determine the effective potentials and nonadiabatic couplings in Eq. (1): $W_{\nu\nu} = U_\nu - Q_{\nu\nu}/2\mu$ and $W_{\nu\nu'} = -[P_{\nu\nu'} d/dR + Q_{\nu\nu'}]/2\mu$, where $P_{\nu\nu'} = \langle \Phi_\nu | d/dR | \Phi_{\nu'} \rangle$ and $Q_{\nu\nu'} = \langle \Phi_\nu | d^2/dR^2 | \Phi_{\nu'} \rangle$. We find $\Phi_\nu(R; \Omega)$ variationally by expanding in exact eigenfunctions of Eq. (2) at large and small R [8]. At ultracold energies the convergence of the scattering observables with respect to the number of basis functions is surprisingly fast [8].

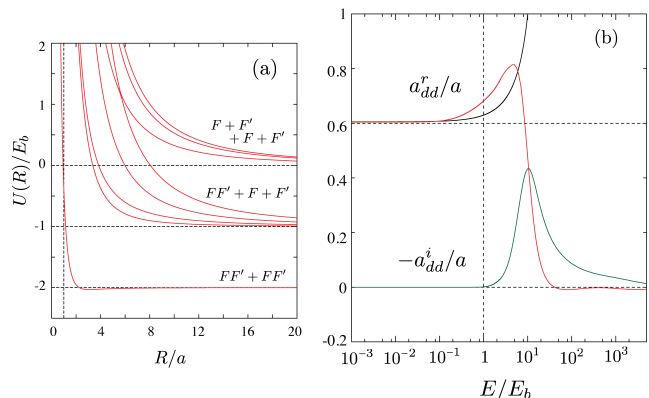


FIG. 2: (color online). (a) Several four-fermion hyperspherical potentials attached to all relevant breakup thresholds are shown. (b) The energy-dependent elastic (red) and inelastic (green) parts of a_{dd} [Eq. (3)] are shown. For energies $E \ll E_b$ we find $a_{dd}^r = 0.605(5)a$ [4], while for $E_{\text{col}} \approx E_b$ finite energy corrections strongly affect a_{dd} . Solid black line: a_{dd} obtained from the effective range expansion [12].

However, including higher order correlations that describe dimer-atom-atom and four free atom configurations is crucial for *accurately* describing scattering processes at *any* collision energy. We find that for $R \lesssim a$ the strongest contribution to the probability density of the dimer-dimer channel function comes from dimer-atom-atom like configurations. Figure 1 shows a graphical representation of this channel function in terms of the internal configuration angles ϕ_1, ϕ_2 and ϕ_3 . The four “cobra”-like surfaces explicitly illustrate the four-fold symmetry ($S_2 \otimes S_2$) of the fermionic problem. The “spines” of the cobras correspond to the interaction valleys where two dissimilar fermions are in close proximity while the “hoods” loosely represent the larger phase-space explored by dimer-atom-atom like configurations.

Figure 2(a) shows the hyperspherical potentials for $a = 125r_0$ showing the full energy landscape with the four-body thresholds for dimer-dimer ($FF' + FF'$), dimer-atom-atom ($FF' + F + F'$), and four atom ($F + F' + F + F'$) collisions. Notice that the four-body potential associated with dimer-dimer collisions is repulsive for $R < a$, in-

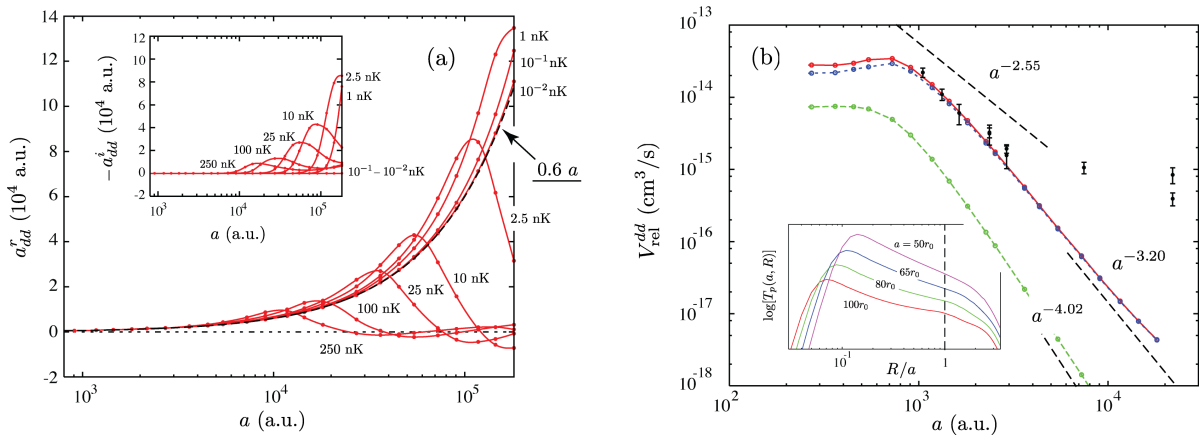


FIG. 3: (color online). (a) The scattering length dependence of a_{dd}^r and a_{dd}^i (inset) at fixed collision energies is shown. At any non-zero collision energy a_{dd} deviates from the zero-energy prediction (black dashed line) as $a \rightarrow \infty$ and strong contributions from molecular dissociation, a_{dd}^i , occur. (b) The dimer-dimer relaxation rate, V_{rel}^{dd} , is shown versus a . The solid line is the total V_{rel}^{dd} and the dashed lines are contributions from different decay pathways (see text). For intermediate a , we reproduce both experimental data [7] (filled circles) and the $a^{-2.55}$ scaling law [4] while deviating from that for larger a . Inset: we show T_p as a function of R for $a = 100r_0$, $80r_0$, $65r_0$, and $50r_0$ (red, green, blue, and magenta respectively).

dicating that zero-energy dimer-dimer elastic scattering must be qualitatively similar to scattering by a hard-sphere of radius a , i.e., $a_{dd}(0) \propto a$. Although a clear and qualitative picture emerges from the four-body potentials alone, we in practice extract scattering observables from coupled-channel solutions to Eq. (1). We define the energy dependent dimer-dimer scattering length, $a_{dd}(E_{col})$, in terms of the complex phase-shift obtained from the corresponding S -matrix element [$S_{dd,dd} = \exp(2i\delta_{dd})$],

$$a_{dd}(E_{col}) = -\frac{\tan \delta_{dd}}{k_{dd}} = a_{dd}^r(E_{col}) + i a_{dd}^i(E_{col}). \quad (3)$$

Here, $k_{dd}^2 = 2mE_{col}$, $E_{col} = E + 2E_b$ is the collision energy and a_{dd}^r and $a_{dd}^i < 0$ are the real and imaginary parts of a_{dd} , representing elastic and inelastic contributions [6].

Figure 2(b) shows a_{dd}^r and a_{dd}^i for $a = 125r_0$. For energies $E_{col} \ll E_b$ we find that $a_{dd}(0) = 0.605(5)a$ in agreement with Refs. [4, 12] while for $E_{col} \lesssim E_b$, although molecular dissociation is still not allowed, i.e. $a_{dd}^i = 0$, we obtain strong corrections to the zero-energy result. At these energies, an effective range expansion, $a_{dd}^{-1}(E_{col}) = a_{dd}^{-1}(0) - \frac{1}{2}r_{dd}k_{dd}^2$ where $r_{dd} = 0.13a$ [12], is accurate over a small range, but quickly fails to reproduce our results [see black solid line in Fig. 2(b)]. For $E_{col} \gtrsim E_b$, the channels for molecular dissociation become open leading to strong inelastic contributions to $a_{dd}(E_{col})$, as parametrized by a_{dd}^i . Our results indicate that both a_{dd}^r and a_{dd}^i are universal functions of energy and scattering length, i.e., insensitive to the details of the short-range physics, which should extend up to $E_{col} \ll 1/mr_0^2$ in the absence of deeply bound states. Due to the small number of basis functions used in these calculations, our results for $E_b \ll E_{col} \ll 1/(mr_0^2)$ are not fully converged, but we expect their qualitative behavior, i.e., the sharp decrease in $a_{dd}(E_{col})$, to persist.

Figure 3(a) demonstrates that when approaching the Feshbach resonance ($a \rightarrow \infty$) at any finite collision energy, molecular dissociation becomes increasingly more important and a_{dd}^r substantially deviates from the zero-energy predictions [black dashed line and inset in Fig. 3(a)]. As $a \rightarrow \infty$, $E_b \propto 1/a^2$ becomes extremely small and such finite energy effects [see Fig. 2(b)] are relevant even at ultracold energies. Therefore, the molecular binding energy E_b , or equivalently $a_c = 1/\sqrt{2\mu_{2b}T}$, defines the range beyond which (i.e., $a > a_c$) deviations from the zero-energy predictions can be observed. Perhaps more importantly, it specifies a regime beyond which molecular dissociation can lead to a long-lived atom-molecule mixture [13, 14], where dimers are continuously converted to atoms and vice-versa, i.e. $FF' + FF' \leftrightarrow FF' + F + F'$. Further, this indicates that the underlying physics of the strongly interacting regime may fundamentally depend on temperature. Values for a_c at 100 nK are 7000 a.u. for ^{40}K and 17000 a.u. for ^6Li , and therefore the finite energy effects above can become experimentally relevant [2].

We also study vibrational relaxation due to dimer-dimer collisions. We verify the suppression of the relaxation rate as $a \rightarrow \infty$, however, with a different a dependence than $a^{-2.55}$ predicted in Ref. [4]. In Ref. [4] it was assumed that the main decay pathway for relaxations is a purely three-body process and requires only three atoms to be enclosed at short distances. Therefore, it neglects the effects of the interaction with the fourth atom. Here, however, we analyze such effects and find that it strongly influences the suppression of relaxation. In our calculations we express the inelastic transitions probability $T_p(a, R)$ in terms of the probability of having three atoms at short distances as a function of the distance $\approx R$ of the fourth atom from the collision center [15]. We calculate T_p from our fully coupled-channel solutions and effective potentials [see Figs. 1 and 2(a)] and

our results are shown in the inset of Fig. 3(b).

In our model the relaxation rate is simply proportional to the transition probability $T_p(a, R)$. It is interesting to note that our formulation allows for the analysis of different decay pathways. For instance, at short distances, $R \approx r_0$, T_p describes inelastic transitions in which *all* four atoms are involved in the collision process. At large distances, $R/a \gg 1$, T_p describes the decay pathway where *only* three atoms participate in the collision, akin to the process studied in Ref. [4]. We note, however, that for values of R up to $R \approx 5$ the scaling law for relaxation depends strongly on R/a and greatly deviates from the $a^{-2.55}$ scaling. In order to take into account inelastic processes for all values of R we define an effective transition probability by integrating $T_p(a, R)$ over R [15]. Our results for the relaxation rate, V_{rel}^{dd} , are shown in Fig. 3(b) where the red solid line is obtained by integrating T_p from $R = 2r_0$ up to $10a$ [16] giving an apparent scaling law of $a^{-3.20 \pm 0.05}$. The dashed lines are obtained from integrating T_p from $R = 2r_0$ to $5r_0$ and from $R = 5r_0$ to $10a$, which yields scaling laws of $a^{-4.02}$ and $a^{-3.20 \pm 0.05}$, respectively, “separating” the contributions from the decay pathways in which four and three atoms participate in the collision process. The amplitudes for each of these contributions, however, are disconnected as they depend on the details of the four- and three-body short-range physics. In contrast, the amplitudes for the $a^{-3.20}$ and $a^{-2.55}$ processes are governed by the same three-body physics. As a result, the fact that we don’t observe the $a^{-2.55}$ scaling implies that it is not important for the range of a used here. The amplitude for the process which leads to the $a^{-2.55}$ scaling is exponentially suppressed owing to the unfavorable overlap of

the dimers’ wavefunction [see inset of Fig. 3(b)]. In fact, for our largest values of a , it is already apparent that in the very large a limit the rate deviates from $a^{-3.20}$, however, to a behavior different than $a^{-2.55}$ [15].

Figure 3(b) rescales our results for V_{rel}^{dd} by an overall constant chosen to fit the experimental data for ^{40}K at a temperature of 70 nK (Regal *et al.* [7]). We note, however, that between $a = 1000$ and 3000 a.u. [17], our results agree with both the experimental data *and* the $a^{-2.55}$ scaling law, approaching our predicted scaling law $a^{-3.20}$ only for larger values of a . This change in behavior of V_{rel}^{dd} originates in the finite range of our model, which represents physics beyond the zero-range model of Ref. [4] where the $a^{-2.55}$ scaling applies for all a .

In summary, we have calculated the energy dependent *complex* dimer-dimer scattering length, $a_{dd}(E_{\text{col}})$, by solving the four-body Schrödinger equation in the adiabatic hyperspherical representation. Our results demonstrate that for experimentally relevant temperatures and scattering lengths the elastic and inelastic contributions of a_{dd} are equally important. We show that molecular dissociation plays an important role and suggest that the many-body behavior in the strongly interacting regime might be significantly altered at finite temperature. Our results also demonstrate a stronger suppression for dimer-dimer relaxation, compared to that obtained in Ref. [4], while remaining consistent with experimental data.

The authors would like to acknowledge D. S. Jin’s group for providing their experimental data, J. von Stecher and D. S. Petrov for fruitful discussions, and the W. M. Keck Foundation for providing computational resources. This work was supported by the National Science Foundation.

-
- [1] D. M. Eagles, Phys. Rev. **186**, 456 (1969); A. J. Leggett, J. Phys. C **41**, 7 (1980); M. Holland *et al.*, Phys. Rev. Lett. **87**, 120406 (2001); E. Timmermans *et al.*, Phys. Lett. A **285**, 228 (2001); Y. Ohashi and A. Griffin, Phys. Rev. Lett. **89**, 130402 (2002).
- [2] C. Chin *et al.*, Science **305**, 1128 (2004); T. Bourdel *et al.*, Phys. Rev. Lett. **93**, 050401 (2004); M. Bartenstein *et al.*, *ibid.* **92**, 120401 (2004); C. A. Regal, M. Greiner, and D. S. Jin, *ibid.* **92**, 040403 (2004); M. W. Zwierlein *et al.*, *ibid.* **92**, 120403 (2004); G. B. Partridge *et al.*, *ibid.* **95** 020404 (2005); M. Bartenstein *et al.*, *ibid.* **92**, 203201 (2004); J. Kinast *et al.*, *ibid.* **92**, 150402 (2004). M. Greiner, C. A. Regal, and D. S. Jin, *ibid.* **94**, 070403 (2005); M. W. Zwierlein, *et al.*, Nature (London) **435**, 1047 (2005).
- [3] P. Pieri and G. C. Strinati, Phys. Rev. B **61**, 15370 (2000).
- [4] D. S. Petrov, C. Salomon, and G. V. Shlyapnikov, Phys. Rev. Lett. **93**, 090404 (2004); Phys. Rev. A **71**, 012708 (2005).
- [5] M. J. Wright *et al.*, Phys. Rev. Lett. **99**, 150403 (2007).
- [6] J. L. Bohn and P. S. Julienne, Phys. Rev. A **56**, 1486 (1997); R. C. Forrey *et al.*, *ibid.* **58**, R2645 (1998).
- [7] J. Cubizolles *et al.*, Phys. Rev. Lett. **91**, 240401 (2003); K. E. Strecker, G. B. Partridge, and R. G. Hulet, *ibid.* **91** 080406 (2003); C. A. Regal, M. Greiner, and D. S. Jin, *ibid.* **92**, 083201 (2004).
- [8] Nirav P. Mehta, Seth T. Rittenhouse, José P. D’Incao, Chris H. Greene, arXiv:0706.1296.
- [9] V. Aquilanti and S. Cavalli. J. Chem. Soc. : Faraday Transactions **95**, 801 (1997); A. Kuppermann. J. Phys. Chem. A **101**, 6368 (1997).
- [10] We omit all reference to the Euler angles because this study treats only the dominant partial wave $J^\pi = 0^+$, where J is the total orbital angular momentum and π is the parity quantum number.
- [11] V. V. Flambaum, G. F. Gribakin, and C. Harabati, Phys. Rev. A **59**, 1998 (1999). The value for r_0 is obtained from the expression $r_0 = 2^{1/2}3^{-1}\Gamma(\frac{1}{4})\Gamma(\frac{3}{4})^{-1}(mC_6)^{1/4}$, Eq. (24), at resonance.
- [12] J. von Stecher, Chris H. Greene, and D. Blume, Phys. Rev. A **76**, 053613 (2007); *ibid.* **77**, 043619 (2008). a_{dd} in these works is calculated to an accuracy similar to our present value.
- [13] S. Jochim *et al.*, Phys. Rev. Lett. **91**, 240402 (2003).
- [14] Y. Shin, A. Schirotzek, C. H. Schunck, and W. Ketterle,

Phys. Rev. Lett. **101**, 070404 (2008).

- [15] See Supplemental Material attached to this file for a more detailed description of our model for dimer-dimer relaxation.
- [16] We have found that integrating T_p from $R = 2r_0$ up to $10a$ is enough to ensure that contributions for $R < 2r_0$

and $R > 10a$ are negligible.

- [17] The experimental data for $a > 3000$ a.u. were taken in the regime where the molecular size is expected to be larger than the interparticle spacing, which prohibits a proper comparison to our results.

Supplemental Material: “Dimer-dimer collisions at finite energies in two-component Fermi gases”

J. P. D’Incao, Seth T. Rittenhouse, N. P. Mehta, and Chris H. Greene
 Department of Physics and JILA, University of Colorado, Boulder, Colorado 80309-0440, USA

In this supplemental material we provide additional details of our model for dimer-dimer relaxation in terms of the transition probability obtained from our numerical calculations [1].

The key observation in our model is that the inelastic transitions leading to deeply bound molecular final states can only occur when *at least* three atoms are enclosed at distances comparable to r_0 . In the hyperspherical representation, the decay pathway in which only three atoms participate is viewed as an infinite series of avoid crossing between the initial dimer-dimer channel and all possible final states, as illustrated in Fig. 1(a), where the red solid curve describe the initial collision channel and the green dashed curves some of the possible final states.

Therefore, for a given a , the inelastic transition to a particular final state can be described in terms of the Fermi Golden rule

$$T_p^{(\lambda)}(a) \propto |\langle \Psi_{dd}(R, \Omega) | V(R, \Omega) | \Psi_\lambda(R, \Omega) \rangle|^2 \quad (1)$$

where Ψ_λ is the final state wave function, labeled by the quantum number λ , Ψ_{dd} is our fully coupled dimer-dimer wavefunction, and V is the sum of the interatomic interactions. The hyperangular behavior of the integrand is assumed to be proportional to the probability amplitude of three particles being in close proximity. On the other hand, the hyperradial behavior of the outgoing channel will oscillate very quickly away from the classical turning point, as shown schematically in Fig. 1(b). The fast oscillation will, in general, cancel out in regions away from the classical turning point, R_λ . This indicates that the integral over the hyperradius will be proportional to the area within the first oscillation of $\Psi_\lambda(R)$ times the remaining hyperradial behavior evaluated at R_λ . Based on these considerations, the squared result yields

$$T_p^{(\lambda)}(a, R_\lambda) \propto \frac{1}{R_\lambda} |F_{dd}(R_\lambda)|^2 \mathcal{F}(R_\lambda), \quad (2)$$

where F_{dd} is the dimer-dimer hyperradial wave function and $\mathcal{F}(R_\lambda)$ is the probability of having three out of four atoms at distances comparable to r_0 at hyperradius R_λ . Therefore, the inelastic transitions to a particular final state λ occurs in the vicinity of R_λ and it is governed by the probability of having the three atoms within distances comparable to r_0 .

In practice, we have calculate $\mathcal{F}(R_\lambda)$ by defining the proximity operator

$$f(R, \Omega) = e^{-(r_{12}^2 + r_{34}^2)/2r_0^2} + \text{cyclic permutaions}, \quad (3)$$

which is non-zero only when three atoms are sufficiently

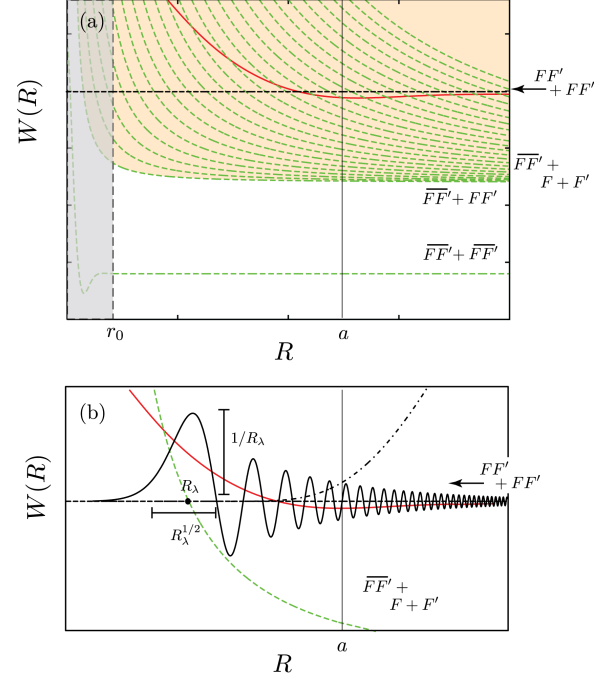


FIG. 1: (color online). (a) A schematic representation of the dimer-dimer relaxation process is shown. The red-solid curve represents the effective potential for the initial dimer-dimer channel, $FF' + FF'$, and green-dashed curves represent the possible final decay channels involving at least one deeply bound molecular state \overline{FF}' . Inelastic transitions to this almost continuum of final states are allowed for all values of R (see main text). (b) Qualitative representations of the behavior of the hyperradial solutions in the dimer-dimer channel (black dot-dashed curve) and in a particular final channel (solid black curve) are shown to illustrate that the inelastic transition is more likely near the classical turning point R_λ .

close to each other. \mathcal{P} is then simply defined as

$$\mathcal{F}(R) \propto \langle \Phi_{dd}(R; \Omega) | f(R, \Omega) | \Phi_{dd}(R; \Omega) \rangle, \quad (4)$$

where Φ_{dd} is our fully coupled dimer-dimer channel function and the integration is taken over all the hyperangles.

Our model for dimer-dimer relaxation, therefore, is simply obtained by summing Eq. (2) over the near continuum of λ states, approximated by an integral over the

classical turning points, which yields

$$\begin{aligned}
 V_{\text{rel}}^{dd} &\propto \frac{1}{k_{dd}} \int T_p^{(\lambda)}(a, R_\lambda) \rho(R) dR \\
 &= \frac{1}{k_{dd}} \int \frac{1}{R_\lambda} |F_{dd}(R_\lambda)|^2 \mathcal{F}(R_\lambda) \rho(R_\lambda) dR_\lambda \\
 &\approx \frac{1}{k_{dd}} \int \frac{P_{\text{WKB}}(R_\lambda) \mathcal{F}(R_\lambda)}{R_\lambda \kappa(R_\lambda)} \rho(R_\lambda) dR_\lambda, \quad (5)
 \end{aligned}$$

where $k_{dd}^2 = 2m(E + 2E_b)$, $\rho(R_\lambda)$ is the nearly constant density of states and $|F_{dd}(R_\lambda)|^2$ was approximated by the WKB wavefunction in the classically forbidden region, $|F_{dd}(R_\lambda)|^2 \approx P_{\text{WKB}}(R_\lambda)/\kappa(R_\lambda)$. Here, P_{WKB} is the WKB tunneling probability for the dimer-dimer hyperradial wavefunction and $\kappa^{\text{WKB}}(R_\lambda)$ is the WKB wavenumber.

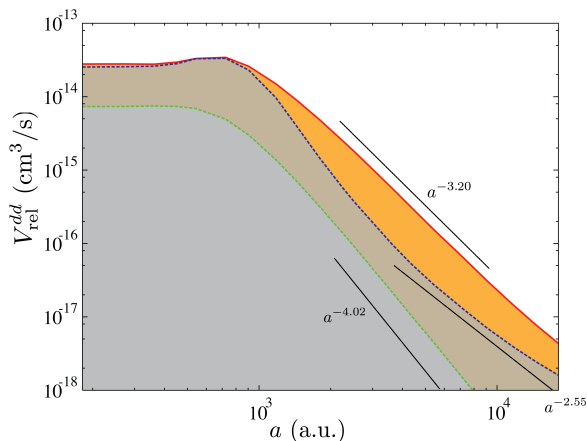


FIG. 2: (color online). The vibrational relaxation rate for different decay pathways is shown. The red-solid curve is the total rate given by Eq. (5), the green-dashed curve is the contribution from short-range inelastic transitions where all four-atoms participate in the collision. The blue-dashed curve is the contribution from inelastic transitions near $R = a$ involving only three-atoms illustrating the effects due to the presence of the fourth atom (see main text).

In our model for relaxation, breaking up the integration over $T_p(a)$ [Eq. (5)] allows us to analyze the contributions from different pathways. In Fig. 2 we show the total rate as a solid-red curve, obtained by integrating Eq. (5) from $2r_0$ to $10a$ [2]. In addition to that, we also plot the results for V_{rel}^{dd} obtained by integrating Eq. (5) from $2r_0$ to $5r_0$, see green-dashed curve in Fig. 2. This result determines the contribution from inelastic transitions which occur predominantly when all four atoms are within distances comparable to r_0 . The blue-dashed curve in Fig. 2, however, shows our results obtained by integrating from a to $4a$, determining the behavior of the contributions from inelastic transitions that occurs near $R = a$. The main difference between this contribution and the total rate comes from the inelastic transitions for $R < a$. Although numerically we are unable to go to larger values of a , it is clear that the contributions for transitions near $R = a$ becomes increasingly more important and in the very large a limit we expect these contributions to dominate the total rate. Interestingly, for the values of a we studied, the contribution for transitions near $R = a$ already falls off slower than the $a^{-2.55}$ prediction of Ref. [3]. Therefore, we conclude that the mechanism that leads to the $a^{-2.55}$ suppression, although, qualitatively correct, doesn't quantitatively describe the transitions near $R = a$ due to the presence of the fourth atom.

[1] See “Dimer-dimer collisions at finite energies in two-component Fermi gases”, J. P. D’Incao, Seth T. Rittenhouse, N. P. Mehta, Chris H. Greene, arXiv:0806.3062
 [2] We have found that integrating out T_p from $R = 2r_0$ up to $10a$ is enough to ensure that contributions for $R < 2r_0$

and $R > 10a$ are negligible.
 [3] D. S. Petrov, C. Salomon, and G. V. Shlyapnikov, Phys. Rev. Lett. **93**, 090404 (2004); Phys. Rev. A **71**, 012708 (2005).